

Dynamic Analysis of Ferroelectric Negative Capacitance - Electrostatic MEMS Hybrid Actuator

Raghuram.T.R and Arvind Ajoy

Abstract—Electrostatic Micro-Electro Mechanical Systems (MEMS) actuators are a key element in today’s electronic switching applications. One of the main challenges in realizing a heterogeneous system having such MEMS actuators along with other CMOS devices is the high operating voltage of the MEMS actuator. In this work, we propose a SPICE based framework to model ferroelectric negative capacitance - electrostatic MEMS hybrid actuators. Using this framework, we demonstrate that the negative capacitance of the ferroelectric can result in a significant reduction in the dynamic pull-in and pull-out voltages of the actuator. We also show the effect of ferroelectric thickness on these voltages and the effect of ferroelectric damping on the energy dissipation. Our proposal shows that the hybrid actuator is better than the standalone MEMS actuator in terms of voltage requirement and energy dissipation. We also reveal the trade-off between the operating voltage and the pull-in time.

Index Terms—Ferroelectric negative capacitance, electrostatic MEMS actuator, dynamic pull-in, SPICE modeling.

I. INTRODUCTION

MICRO Electro Mechanical Systems (MEMS) based on electrostatic actuation and sensing are an integral part of today’s electronics. The ITRS roadmap describes the significance of many such devices in applications ranging from consumer - to - automotive - to - medical electronics [1]. Electrostatic MEMS actuators are very popular and are widely used because of their inherent low power consumption. The response of such electrostatic MEMS actuators to voltage excitation is typically classified into two: static and dynamic [2]–[6]. The former corresponds to the input voltage being varied slowly, so that the actuator is in quasi-static equilibrium. The latter corresponds to the input voltage being varied suddenly, as in the case of a step voltage excitation. Electrostatic actuators with step voltage excitation (dynamic) play a key role in switching (like RF MEMS switches) and display applications [7]–[11]. However, the operating voltages of such electrostatic MEMS actuators are typically much larger than the supply voltages used in modern CMOS integrated circuits. Realization of low-voltage electrostatic MEMS switches will enable a seamless integration of MEMS with CMOS electronics.

A novel technique to realize low-voltage electrostatic MEMS actuators was proposed and its static response was analyzed analytically in Ref. [12]. The idea was to connect a ferroelectric capacitor exhibiting negative capacitance in series with the MEMS actuator, thus forming a ferroelectric negative

Raghuram.T.R is with the Department of Electrical Engineering, Indian Institute of Technology Palakkad, Palakkad, India. e-mail: 121704004@smail.iitpkd.ac.in

Arvind Ajoy is with the Department of Electrical Engineering, Indian Institute of Technology Palakkad, Palakkad, India. e-mail: arvindajoy.iitpkd.ac.in

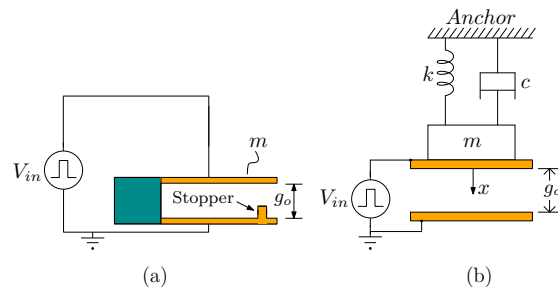


Fig. 1. An example of modeling a generic electrostatic MEMS actuator using a 1-DOF model. (a) Cantilever MEMS (b) Equivalent 1-DOF model capturing the essential features of the cantilever structure.

capacitance - electrostatic MEMS hybrid actuator. Dynamic pull-in is however more relevant for switching applications than static analysis. To the best of our knowledge, dynamic pull-in of these hybrid actuators has not yet been reported.

In this work, we model the hybrid actuator numerically using SPICE and analyze the dynamic response. SPICE based modeling is circuit compatible and thus it can facilitate evaluation of circuit performance of various heterogeneous CMOS-MEMS systems easily. Using this approach, we demonstrate sub 1V dynamic operation of the hybrid actuator, enabling the integration of such MEMS actuators with modern CMOS devices. This eliminates the need of additional on-chip voltage sources and drive electronics used in present day MEMS-CMOS hybrid integrated circuits [13]–[16]. This also eliminates the scaling down of the structural parameters of the MEMS actuator to achieve low-voltage operation [17]–[19]. With this model, the effect of ferroelectric thickness on the operating voltage is illustrated. Further, the effect of ferroelectric damping and the pull-in time analysis are also presented.

This paper is organized as follows. Section II reviews the dynamics of standalone electrostatic MEMS actuator. Section III presents the modeling of ferroelectric negative capacitance - electrostatic MEMS hybrid actuator using SPICE. Simulation results and discussion are detailed in section IV. Section V presents our conclusion.

II. REVIEW OF DYNAMICS OF ELECTROSTATIC MEMS ACTUATOR

In this work, we model a generic standalone electrostatic MEMS actuator as a single degree of freedom (1-DOF), parallel plate arrangement consisting of a pair of electrodes separated by an airgap g_o . As shown in the Fig. 1, one electrode (bottom) is fixed and the other (top) is movable. The parameters used in the 1-DOF model (mass m , spring

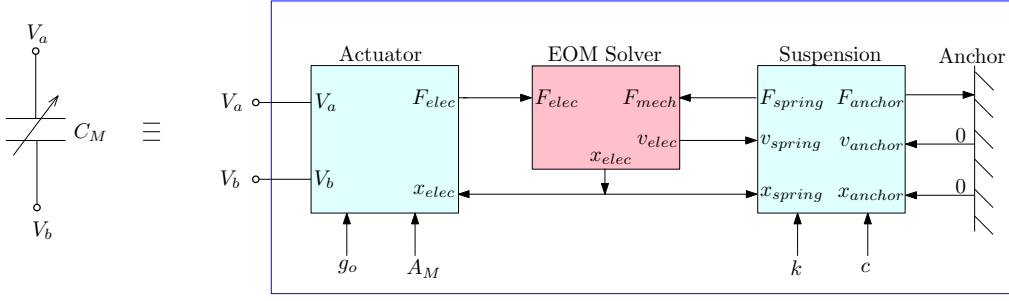


Fig. 2. SPICE model of standalone electrostatic MEMS actuator. Arrows pointing into (out of) a block refer to inputs (outputs) to (from) the block. x designates position, v designates velocity and F designates forces. Implementation of these blocks using circuit elements follows Ref. [20].

constant k , damping coefficient c) represent their effective equivalents in the generic actuator. In this work, we set the damping coefficient to zero, so as to enable a comparison with analytical results wherever possible. For dynamic operation, a step voltage is applied to the actuator. Below a certain value of this applied step voltage, called the dynamic pull-in voltage, the response of the actuator is periodic. The maximum value of this periodic displacement of the electrode is called dynamic pull-in displacement. For applied step voltage above the dynamic pull-in voltage, the movable top electrode snaps down onto the bottom electrode. This condition is called dynamic pull-in [5]. After achieving pull-in, when the applied step voltage is decreased to a specific value, called the dynamic release voltage / pull-out voltage, the pull-in condition is lost and the movable electrode comes back to its original position.

The equation of motion governing the actuator response to the applied voltage $V_{in} u(t)$, where $u(t)$ is the unit step function, is given by

$$m \frac{d^2 x}{dt^2} + c \frac{dx}{dt} + k x = \frac{\epsilon_o A_M V_{in}^2}{2 (g_o - x)^2} \quad (1)$$

for $t \geq 0$. A_M is the area of the electrode, ϵ_o is the permittivity of free space, and x is the dynamic variable representing the displacement of the electrode. With damping neglected, the dynamic pull-in voltage V_{PI} and the dynamic pull-in displacement X_{PI} are given by [11]

$$V_{PI} = \sqrt{\frac{k g_o^3}{4 \epsilon_o A_M}} \quad \text{and} \quad X_{PI} = \frac{g_o}{2} \quad (2)$$

Note that no analytical expression for dynamic release voltage has been reported in literature.

III. MODELING FERROELECTRIC NEGATIVE CAPACITANCE - ELECTROSTATIC MEMS HYBRID ACTUATOR

The SPICE model of the standalone electrostatic MEMS is implemented as shown in Fig. 2. It consists of four modules namely the actuator, the suspension, the Equation of Motion (EOM) solver and the anchor [20]. These modules are represented as sub-circuits in the schematic along with their associated parameters as depicted in Fig. 2. The initial displacement and velocity of the movable electrode are taken as zero. The actuator module takes the applied step voltage V_{in} , area A_M , initial air-gap g_o and the electrode displacement x_{elec} as input parameters and calculates the electrostatic force

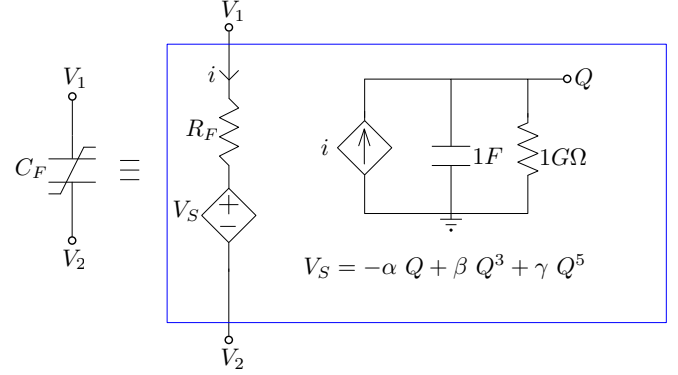


Fig. 3. SPICE model of ferroelectric capacitor. The charge Q is determined using an RC integrator. The voltage source V_S is implemented using arbitrary behavioral voltage source.

$F_{elec} = \epsilon_o A_M V_{in}^2 / 2 (g_o - x)^2$. The suspension module takes the electrode displacement x_{elec} , electrode velocity v_{elec} , the spring constant k and the damping coefficient c as the input parameters and calculates the mechanical restoring force $F_{mech} = c \cdot dx/dt + kx$. The EOM solver module is placed between the actuator and suspension modules. The EOM solver compares the two forces F_{elec} and F_{mech} and calculates the resultant electrode displacement and velocity by solving Eq. (1) for the specified electrode mass m . Electrical feedback connection is provided within these blocks to reach the equilibrium solution of the electrode displacement numerically for the applied step voltage.

The dynamics of the ferroelectric capacitor (single domain) is captured by the time dependent Landau - Khalatnikov (LK) equation [21]–[26] relating the voltage V_F across the ferroelectric to charge Q as

$$V_F = -\alpha Q + \beta Q^3 + \gamma Q^5 + R_F \frac{dQ}{dt} \quad (3)$$

$$\alpha = -\frac{\alpha_F t_F}{A_F}; \quad \beta = \frac{\beta_F t_F}{A_F^3}; \quad \gamma = \frac{\gamma_F t_F}{A_F^5}; \quad R_F = \frac{\rho t_F}{A_F} \quad (4)$$

where ρ is the ferroelectric damping constant; α_F , β_F and γ_F are ferroelectric anisotropy coefficients, t_F is the thickness of the ferroelectric, and A_F is the area of the ferroelectric. The last term of Eq. (3) denotes the voltage drop across resistor R_F with dQ/dt representing the current i through it. Thus, Eq. (3) is implemented in SPICE as a Voltage Controlled Voltage

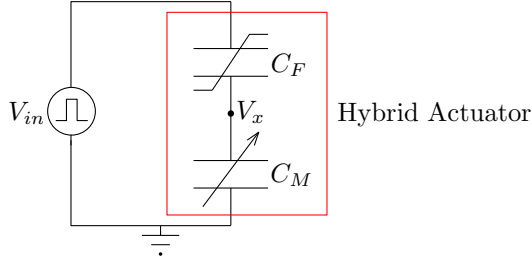


Fig. 4. Ferroelectric negative capacitance -electrostatic MEMS hybrid actuator equivalent circuit. C_F represents the ferroelectric capacitor and C_M represents the variable capacitance provided by the MEMS actuator.

Source (VCVS) in series with resistor R_F . The SPICE model of the ferroelectric capacitor is shown in Fig. 3. The charge Q is estimated by integrating the current i through the capacitor [27].

The ferroelectric negative capacitance - electrostatic MEMS hybrid actuator is modeled in SPICE by cascading a ferroelectric capacitor C_F with the standalone MEMS actuator (depicted as a variable capacitor C_M) as shown in Fig. 4. The intermediate node voltage V_x is obtained as

$$V_x = V_{in} \frac{C_F}{C_F + C_M} \quad (5)$$

Since the ferroelectric capacitor offers negative capacitance, Eq. (5) can be rewritten as

$$V_x = V_{in} \frac{|C_F|}{|C_F| - C_M} \quad (6)$$

When the absolute value of ferroelectric capacitance $|C_F|$ is close to the MEMS capacitance C_M , the intermediate node voltage shows voltage amplification. Thus the MEMS actuator requires a reduced voltage to achieve pull-in. This is the key principle behind reduction in the dynamic pull-in voltage of the electrostatic MEMS actuator in the presence of a series ferroelectric capacitor.

IV. SIMULATION RESULTS AND DISCUSSION

Table I. lists the parameters of the hybrid actuator used in the simulation. The ferroelectric layer thickness and area are designed so as to obtain a static pull-in voltage of 0.8V and a static pull-out voltage of 0V, using the equations available in Ref. [12]. The validation of the SPICE model for the static pull-in and pull-out analysis can be found in the Appendix. The movement of the top electrode is limited by means of a stopper of height h_s .

The standalone MEMS model is simulated first to obtain the dynamic response as shown in Fig. 5. Clearly, for input step voltage less than the dynamic pull-in voltage (18.67 V), the actuator response is periodic. For input step voltage greater than the dynamic pull-in voltage, the actuator achieves pull-in as predicted by theory in Eq. (2). A release voltage of 17.99 V is obtained from simulation. The ferroelectric capacitor model is now connected in series to the standalone MEMS model to form the hybrid actuator. SBT ($Sr_{0.8}Bi_{2.2}Ta_2O_9$)

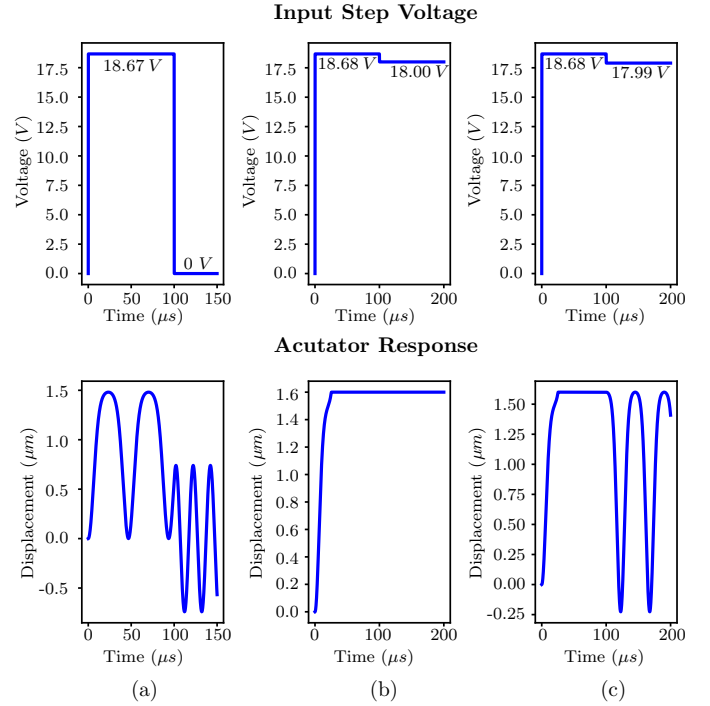


Fig. 5. Standalone electrostatic MEMS actuator dynamic response (a) Actuator response before dynamic pull-in. (b) Actuator response after dynamic pull-in and without release. (c) Actuator response after dynamic pull-in and with release.

is used as the ferroelectric material. Again, the dynamic response of the hybrid actuator is obtained by applying a step input voltage as shown in Fig. 6. The dynamic pull-in and release voltages of the hybrid actuator are found to be 0.66 V and 0.01 V respectively. Compared to the standalone MEMS actuator, there is a significant reduction in the operating voltages of the hybrid actuator. This is because of the voltage amplification due to the negative capacitance of the series ferroelectric capacitor. This sub 1V operation of the hybrid actuator allows seamless integration of such MEMS

TABLE I
FERROELECTRIC NEGATIVE CAPACITANCE - ELECTROSTATIC MEMS
HYBRID ACTUATOR PARAMETERS FOR SPICE SIMULATION

Parameter	Value
Length of the cantilever, L	160 μm
Width of the cantilever, W	6 μm
Thickness of the cantilever, T	2 μm
Cantilever Material	Silicon (Si)
Young's Modulus, E	150 GPa
Density, D	2330 kg/m^3
Mass, m	4.4736 $\times 10^{-12}$ kg
Spring Constant, k	0.439 N/m
Initial air-gap, g_o	3 μm
Stopper height, h_s	1.4 μm
Permittivity of free space, ϵ_o	8.854 $\times 10^{-12}$ F/m
Ferroelectric Material	SBT ($Sr_{0.8}Bi_{2.2}Ta_2O_9$) [12]
α_F	-6.5 $\times 10^7$ m/F
β_F	3.75 $\times 10^9$ $\text{m}^5/\text{F}/\text{C}^2$
γ_F	0 $\text{m}^9/\text{F}/\text{C}^4$
Ferroelectric Thickness, t_F	5.99 μm
Ferroelectric Area, A_F	1.1659 $\times 10^{-12}$ m^2

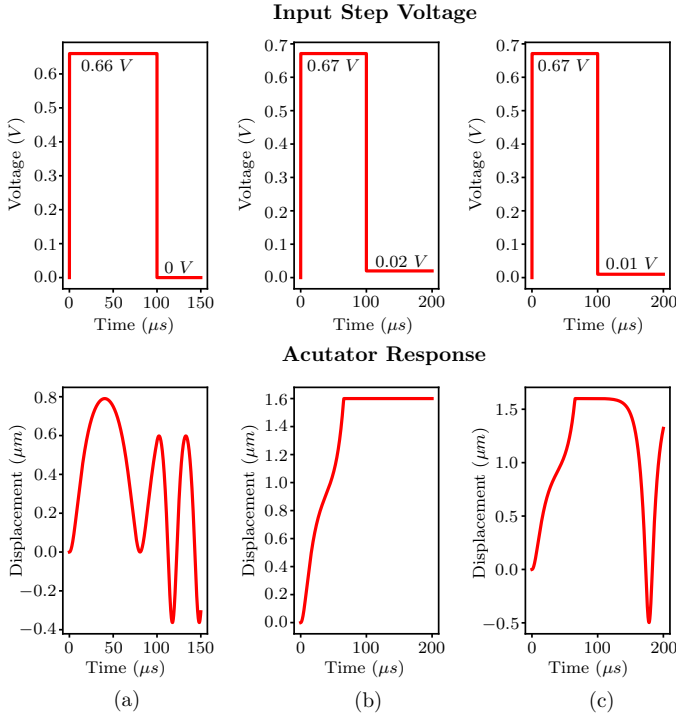


Fig. 6. Ferroelectric negative capacitance - electrostatic MEMS hybrid actuator dynamic response showing significant reduction in operating voltages. (a) Actuator response before dynamic pull-in. (b) Actuator response after dynamic pull-in and without release. (c) Actuator response after dynamic pull-in and with release.

actuators with modern CMOS devices and thus eliminating the need of any drive electronics or additional on-chip voltage up-converters. This also eliminates the need to scale down the structural parameters of the MEMS actuator to achieve low-voltage operation. Electrostatic MEMS actuators are inherently low-power devices owing to their near zero power dissipation [28], [29]. Reduction in the operating voltages further reduces the power dissipation during switching and thus enabling the use of such actuators in low-power, low-voltage applications.

The effect of ferroelectric thickness t_F on the dynamic

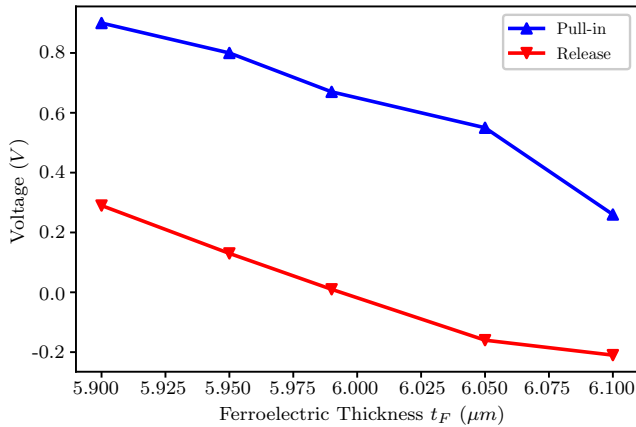


Fig. 7. Effect of ferroelectric thickness t_F on the dynamic pull-in and release voltage of the hybrid actuator depicting the possibility of obtaining both positive and negative release voltages by proper choice of ferroelectric thickness.

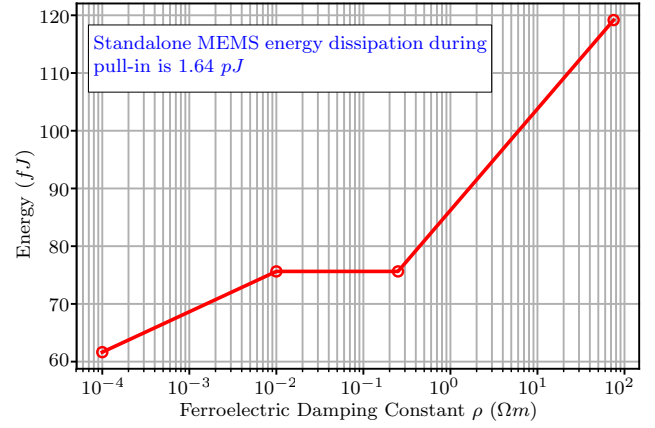


Fig. 8. Effect of ferroelectric damping constant ρ on the energy dissipation during dynamic pull-in in the hybrid actuator. Note that there is one order reduction in the energy dissipation in comparison with the standalone MEMS actuator due to reduction in the pull-in voltage.

pull-in and release voltage is shown in Fig. 7. Increase in the ferroelectric thickness reduces the operating voltages. This is because, with increase in ferroelectric thickness, the ferroelectric capacitance decreases leading to enhanced voltage amplification. This is in agreement with a similar trend observed in ferroelectric negative capacitance - FET devices [24] where the gate voltage reduces with increase in ferroelectric thickness. However, the ferroelectric thickness should be properly chosen so as to preserve the voltage amplification phenomenon. Tailoring ferroelectric thickness t_F can also ensure 0 V release voltage facilitating the use of single sub 1V voltage source for both pull-in and release. For example, with t_F as 5.95 μm , after achieving dynamic pull-in, a 0 V step voltage will result in the release of the electrode. Another feature of this hybrid actuator is that the release voltage can be made negative as evident from Fig. 7. Negative release voltage is favourable for bipolar voltage actuation of electrostatic MEMS actuators leading to improved reliability [30], [31] and also in memory applications [32]. Thus, it is possible to have both positive and negative release voltages by carefully choosing the ferroelectric thickness.

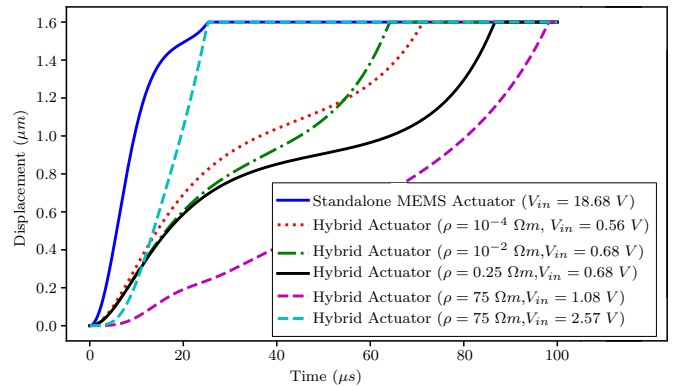


Fig. 9. Dynamic pull-in time analysis of standalone MEMS actuator and hybrid actuator. It is shown that the hybrid actuator is slower in comparison with the standalone MEMS actuator to achieve dynamic pull-in. There also exists a trade-off between the applied step voltage and the pull-in time.

The effect of ferroelectric damping is captured by the resistance R_F in the SPICE model of the ferroelectric capacitor. The effect of ferroelectric damping constant ρ on the energy dissipated during pull-in is shown in Fig. 8. Large range of ρ is used in the simulation for a comprehensive prognosis. The energy dissipated during pull-in in the standalone MEMS actuator is 1.64 pJ . The energy dissipation during pull-in in the hybrid actuator for different values of ρ is of the order of fJ . For example, for $\rho = 75 \text{ } \Omega m$, the energy dissipated during pull-in is 119.17 fJ . This shows one order reduction in the energy dissipation in the hybrid actuator. This is a direct consequence of the reduction in the dynamic pull-in voltage of the actuator. As long as the equivalent series capacitance C_{eq} of the hybrid actuator ($C_{eq}^{-1} = C_F^{-1} + C_M^{-1}$) remains positive, the hybrid actuator will behave like a positive capacitor and C_{eq} will be larger than both C_F and C_M . Thus the energy dissipated during switching (energy $\propto 1/C_{eq}$) will be much smaller than that of the standalone MEMS actuator. The energy dissipation has a strong dependency on the ferroelectric damping constant ρ . The energy dissipation increases with increase in ρ . As long as ρ of the ferroelectric is such that the energy dissipated in the hybrid actuator is less than that of the standalone MEMS actuator, the ferroelectric material is good enough to be employed in the hybrid actuator. This result should motivate development of fabrication techniques that yield ferroelectrics with minimum ferroelectric damping constant.

The dynamic pull-in time analysis of standalone MEMS actuator and the hybrid actuator is shown in Fig. 9. The release time analysis is not considered as displacement by only few nanometers is sufficient to release the electrode. It is observed that the hybrid actuator is slower in comparison with the standalone MEMS actuator to achieve dynamic pull-in due to the addition of the series ferroelectric capacitor. There is also a trade-off between the applied step input voltage and the pull-in time. Larger step input voltage will result in faster pull-in of the actuator. This suggests that, by applying a slightly higher step voltage (which is still smaller than that of the standalone actuator), the pull-in time of the hybrid actuator can be made equal to the pull-in time of the standalone actuator. This ensures low-voltage operation of the hybrid actuator without compromising on the pull-in time. For example, standalone MEMS actuator and hybrid actuator with $\rho = 75 \text{ } \Omega m$ and step input voltage $V_{in} = 2.57 \text{ V}$ will have the same dynamic pull-in time as depicted in Fig. 9.

V. CONCLUSION

The dynamic analysis of ferroelectric negative capacitance - electrostatic MEMS hybrid actuator based on SPICE multi-physics model is presented in this work. It is shown that the dynamic pull-in and release voltage of this hybrid actuator is significantly reduced due to the presence of the series ferroelectric capacitor. This allows straightforward integration of such actuators with modern CMOS devices. Further, this also opens the door for the use of such actuators in low-power, low-voltage applications. The effect of ferroelectric thickness in achieving both positive and negative release voltage is also

illustrated. The effect of ferroelectric damping on the energy dissipation reveals that there is considerable reduction in the energy dissipation in the hybrid actuator in comparison with the standalone MEMS actuator as long as the ferroelectric damping constant is low. The pull-in time analysis shows that there is a trade-off between the applied step voltage and the dynamic pull-in time. Finally, since the model is SPICE based and thus circuit compatible, this can be used in conjunction with other low-voltage CMOS circuits to realize various heterogeneous CMOS - MEMS systems.

APPENDIX

The static pull-in voltage V_{SPI} and the travel range X_{Tr} of the hybrid actuator is given by

$$V_{SPI} = r_{\alpha N} \sqrt{\frac{r_{\alpha N}}{r_{\beta N}}} \sqrt{\frac{8 k g_o^3}{27 \epsilon_o A_M}}; X_{Tr} = \left(\frac{r_{\alpha N}}{r_{\beta N}}\right) \left(\frac{g_o}{3}\right) \quad (\text{A1})$$

where

$$r_{\alpha N} = 1 - \frac{t_F A_M |\alpha_F| \epsilon_o}{g_o A_F}; r_{\beta N} = 1 - \left[(2 \beta_F k \epsilon_o^2) \left(\frac{t_F A_M^2}{A_F^3} \right) \right] \quad (\text{A2})$$

Assuming zero static release voltage, we have $g_o - h_s = (r_{\alpha N}/r_{\beta N}) g_o$. Thickness t_F and area A_F are calculated so as to obtain $V_{SPI} = 0.8 \text{ V}$. The static pull-in and release characteristics of the hybrid actuator is shown in Fig. A1. The simulation results are in agreement with the analytical results given in Ref. [12], thus validating the hybrid actuator SPICE model.

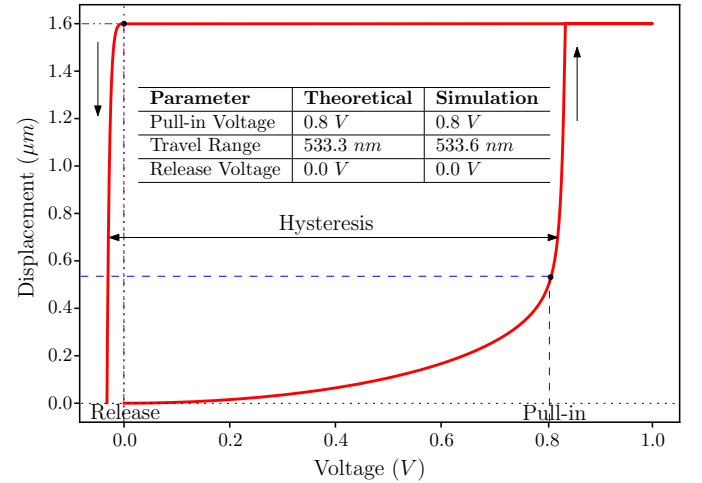


Fig. A1. Static pull-in and release characteristics of the hybrid actuator. The simulation results are in agreement with the analytical results given in Ref. [12], thus validating the hybrid actuator SPICE model.

ACKNOWLEDGEMENT

The authors thank Dr. Revathy Padmanabhan and Dr. Sukomal Dey, Indian Institute of Technology Palakkad for helpful discussions.

REFERENCES

- [1] "2015 International Technology Roadmap for Semiconductors (ITRS)," Tech. Rep., Jun. 2015.
- [2] M. I. Younis, *MEMS Linear and Nonlinear Statics and Dynamics*. Boston, MA: Springer US, 2011, vol. 20, doi:10.1007/978-1-4419-6020-7.
- [3] L. A. Rocha, E. Cretu, and R. F. Wolffenbuttel, "Pull-in dynamics: Analysis and modeling of the transitional regime," in *Proc. 17th IEEE Int. Conf. MEMS*, Jan. 2004, pp. 249–252, doi:10.1109/MEMS.2004.1290569.
- [4] D. Elata, "On the static and dynamic response of electrostatic actuators," *Bull. Polish Acad. Sci.*, vol. 53, no. 4, pp. 373–384, Dec. 2005.
- [5] V. Leus and D. Elata, "On the dynamic response of electrostatic MEMS switches," *J. Microelectromech. Syst.*, vol. 17, no. 1, pp. 236–243, Feb. 2008, doi:10.1109/JMEMS.2007.908752.
- [6] W.-M. Zhang, H. Yan, Z.-K. Peng, and G. Meng, "Electrostatic pull-in instability in MEMS/NEMS: A review," *Sens. Actuators A, Phys.*, vol. 214, pp. 187–218, Aug. 2014, doi:10.1016/j.sna.2014.04.025.
- [7] G. N. Nielson and G. Barbastathis, "Dynamic pull-in of parallel-plate and torsional electrostatic MEMS actuators," *J. Microelectromech. Syst.*, vol. 15, no. 4, pp. 811–821, Aug. 2006, doi:10.1109/JMEMS.2006.879121.
- [8] G. N. Nielson, R. H. Olsson, G. R. Bogart, P. R. Resnick, O. B. Spahn, C. Tigges, G. Grossetete, and G. Barbastathis, "Dynamic pull-in and switching for sub-pull-in voltage electrostatic actuation," in *Proc. 14th Int. Conf. Solid-State Sens., Actuators, Microsyst. (TRANSDUCERS)*, Jun. 2007, pp. 455–459, doi:10.1109/SENSOR.2007.4300166.
- [9] S. Shekhar, K. J. Vinoy, and G. K. Ananthasuresh, "Switching and release time analysis of electrostatically actuated capacitive RF MEMS switches," *Sens. Transducers*, vol. 130, no. 7, pp. 77–90, Jul. 2011.
- [10] G. M. Rebeiz, *RF MEMS: Theory, Design, and Technology*. John Wiley & Sons, 2004.
- [11] K. B. Lee, *Principles of Microelectromechanical Systems*. John Wiley & Sons, 2011.
- [12] M. Masduzzaman and M. A. Alam, "Effective nanometer airgap of NEMS devices using negative capacitance of ferroelectric materials," *Nano Lett.*, vol. 14, no. 6, pp. 3160–3165, May 2014, doi:10.1021/nl5004416.
- [13] G. M. Rebeiz, "RF MEMS switches: Status of the technology," in *Proc. 12th Int. Conf. Solid-State Sens., Actuators, Microsyst. (TRANSDUCERS)*, vol. 2, Jun. 2003, pp. 1726–1729, doi:10.1109/SENSOR.2003.1217118.
- [14] N. Dumas, L. Latorre, F. Mailly, and P. Nouet, "Design of a smart CMOS high-voltage driver for electrostatic MEMS switches," in *Symp. Design Test Integration and Packag. of MEMS/MOEMS (DTIP)*, May 2010, pp. 44–47.
- [15] J. F. Saheb, J. F. Richard, M. Sawan, R. Meingan, and Y. Savaria, "System integration of high voltage electrostatic MEMS actuators," *Analog Integr. Circ. and Sig. Process.*, vol. 53, no. 1, pp. 27–34, Oct. 2007, doi:10.1007/s10470-006-9020-x.
- [16] J. A. Brandt, "High voltage bias waveform generator for an RF MEMS microswitch," Master's thesis, University of New Hampshire, Durham, 2008.
- [17] J. O. Lee, Y.-H. Song, M.-W. Kim, M.-H. Kang, J.-S. Oh, H.-H. Yang, and J.-B. Yoon, "A sub-1-volt nanoelectromechanical switching device," *Nature Nanotechnol.*, vol. 8, no. 1, pp. 36–40, Jan. 2013, doi:10.1038/nnano.2012.208.
- [18] W. W. Jang, J. O. Lee, J.-B. Yoon, M.-S. Kim, J.-M. Lee, S.-M. Kim, K.-H. Cho, D.-W. Kim, D. Park, and W.-S. Lee, "Fabrication and characterization of a nanoelectromechanical switch with 15-nm-thick suspension air gap," *Appl. Phys. Lett.*, vol. 92, no. 10, p. 103110, Mar. 2008, doi:10.1063/1.2892659.
- [19] A. Attaran and R. Rashidzadeh, "Ultra low actuation voltage RF MEMS switch," *Micro and Nano Syst. Lett.*, vol. 3, no. 1, pp. 1–4, Dec. 2015, doi:10.1186/s40486-015-0024-0.
- [20] H. Toshiyoshi, "A SPICE-based multi-physics simulation technique for integrated MEMS," in *IEEE Int. Conf. Simulation of Semiconductor Processes and Devices*, Sep. 2011, pp. 239–242, doi:10.1109/SISPAD.2011.6035069.
- [21] S. Salahuddin and S. Datta, "Use of negative capacitance to provide voltage amplification for low power nanoscale devices," *Nano Lett.*, vol. 8, no. 2, pp. 405–410, Feb. 2008, doi:10.1021/nl071804g.
- [22] A. I. Khan, K. Chatterjee, B. Wang, S. Drapcho, L. You, C. Serrao, S. R. Bakaul, R. Ramesh, and S. Salahuddin, "Negative capacitance in a ferroelectric capacitor," *Nature Mater.*, vol. 14, no. 2, pp. 182–186, Feb. 2015, doi:10.1038/nmat4148.
- [23] A. Aziz, S. Ghosh, S. Datta, and S. K. Gupta, "Physics-based circuit-compatible SPICE model for ferroelectric transistors," *IEEE Electron Device Lett.*, vol. 37, no. 6, pp. 805–808, Jun. 2016, doi:10.1109/LED.2016.2558149.
- [24] Y. Li, K. Yao, and G. S. Samudra, "Delay and power evaluation of negative capacitance ferroelectric MOSFET based on SPICE model," *IEEE Trans. Electron Devices*, vol. 64, no. 5, pp. 2403–2408, May 2017, doi:10.1109/TED.2017.2674020.
- [25] Y. Li, Y. Kang, and X. Gong, "Evaluation of negative capacitance ferroelectric MOSFET for analog circuit applications," *IEEE Trans. Electron Devices*, vol. 64, no. 10, pp. 4317–4321, Oct. 2017, doi:10.1109/TED.2017.2734279.
- [26] A. I. Khan, "Negative capacitance for ultra-low power computing," Ph.D. dissertation, UC Berkeley, 2015.
- [27] M. Pešić, C. Künneth, M. Hoffmann, H. Mulaosmanovic, S. Müller, E. T. Breyer, U. Schroeder, A. Kersch, T. Mikolajick, and S. Slesazek, "A computational study of hafnia-based ferroelectric memories: from ab initio via physical modeling to circuit models of ferroelectric device," *J. Comput. Electron.*, vol. 16, no. 4, pp. 1236–1256, Dec. 2017, doi:10.1007/s10825-017-1053-0.
- [28] E. R. Brown, "RF-MEMS switches for reconfigurable integrated circuits," *IEEE Trans. Microw. Theory Tech.*, vol. 46, no. 11, pp. 1868–1880, Nov. 1998, doi:10.1109/22.734501.
- [29] G. M. Rebeiz and J. B. Muldavin, "RF MEMS switches and switch circuits," *IEEE Microw. Mag.*, vol. 2, no. 4, pp. 59–71, Dec. 2001, doi:10.1109/6668.969936.
- [30] Z. Peng, X. Yuan, J. C. Hwang, D. I. Forehand, and C. L. Goldsmith, "Dielectric charging of RF MEMS capacitive switches under bipolar control-voltage waveforms," in *Proc. IEEE/MTT-S Int. Microw. Symp.*, Jun. 2007, pp. 1817–1820, doi:10.1109/MWSYM.2007.380102.
- [31] M. Domínguez, D. López, D. Molinero, and J. Pons-Nin, "Dielectric charging control for electrostatic MEMS switches," in *Proc. SPIE*, vol. 7679, May 2010, pp. 1–11, doi:10.1117/12.853177.
- [32] W. Y. Choi, T. Osabe, and T.-J. K. Liu, "Nano-Electro-Mechanical nonvolatile memory (NEMory) cell design and scaling," *IEEE Trans. Electron Devices*, vol. 55, no. 12, pp. 3482–3488, Dec. 2008, doi:10.1109/TED.2008.2006540.